A quasi-static model of drop impact

AIP | Physics of Fluids

A quasi-static model of drop impact

Jan Moláček and John W. M. Bush

Citation: Phys. Fluids **24**, 127103 (2012); doi: 10.1063/1.4771607
View online: http://dx.doi.org/10.1063/1.4771607
View Table of Contents: http://pof.aip.org/resource/1/PHFLE6/v24/i12
Published by the American Institute of Physics.

PHYSICS OF FLUIDS **24**, 127103 (2012)

A quasi-static model of drop impact

Jan Moláček[a] and John W. M. Bush[b]
Department of Mathematics, Massachusetts Institute of Technology, 77 Massachusetts Avenue, Cambridge, Massachusetts 02139, USA

(Received 14 July 2012; accepted 16 November 2012; published online 19 December 2012)

We develop a conceptually simple theoretical model of non-wetting drop impact on a rigid surface at small Weber numbers. Flat and curved impactor surfaces are considered, and the influence of surface curvature is elucidated. Particular attention is given to characterizing the contact time of the impact and the coefficient of restitution, the goal being to provide a reasonable estimate for these two parameters with the simplest model possible. Approximating the shape of the drop during impact as quasi-static allows us to derive the governing differential equation for the droplet motion from a Lagrangian. Predictions of the resulting model are shown to compare favorably with previously reported experimental results. © *2012 American Institute of Physics*. [http://dx.doi.org/10.1063/1.4771607]

I. INTRODUCTION

The impact of liquid droplets on solids is important in a variety of industrial and biological processes. Industrial applications include insecticide and pesticide design,[1–3] inkjet printing,[4] and fuel injection, as well as the design of airplane, ship, and windmill blades.[5] For many plants and small creatures, the impact and adherence of a raindrop can lead to tissue damage or other deleterious consequences, such as compromised photosynthesis in the case of plants and respiration in the case of insects; thus, the integument of many plants and insects is hydrophobic.[6,7]

The nature of small droplet collision depends on the wettability of the impacted solid, which will in general depend in turn on its surface chemistry and texture.[8] If the droplet wets the solid, the spreading and detachment of the droplet will depend critically on the contact line dynamics.[9] In the present paper, we consider the case of non-wetting impact, in which a thin air layer is maintained between the droplet and the surface, so that contact line dynamics need not be considered. Such is the case for relatively low-energy impact of drops on super-hydrophobic surfaces,[10] a rigid surface coated with a liquid film[11] or a highly viscous liquid surface.[12]

We further restrict our attention to low-energy impacts in which the droplet deformation remains small, allowing for an analytical treatment. Two key parameters that characterize the impact are the contact time T_C and the coefficient of restitution C_R. The contact time can be defined as the time over which the droplet experiences a reaction force from the impacted object; the coefficient of restitution as the ratio of the normal components of outgoing to incoming velocity: $C_R = \frac{(V_{out})_n}{(V_{in})_n}$. While, strictly speaking, these definitions can only be approximate due to the interaction between drop and impactor via viscous forces in the intervening gas, for the class of problems to be considered, the resulting ambiguity is negligible.

Six physical variables affect the normal impact of a nonwetting drop on a flat rigid surface: the droplet radius R_0 and impact speed V_{in}, the liquid density ρ, dynamic viscosity μ, and surface tension σ and the gravitational acceleration g. These give rise to three nondimensional groups. The Weber number $\mathbb{W}e = \rho R_0 V_{in}^2/\sigma$, Bond number $\mathbb{B}o = \rho g R_0^2/\sigma$, and Ohnesorge number $\mathbb{O}h = \mu\,(\sigma\rho R_0)^{-1/2}$ prescribe the relative magnitudes of, respectively, inertia, gravity, and viscosity to

[a]Electronic mail: molacek@math.mit.edu.
[b]Electronic mail: bush@math.mit.edu.

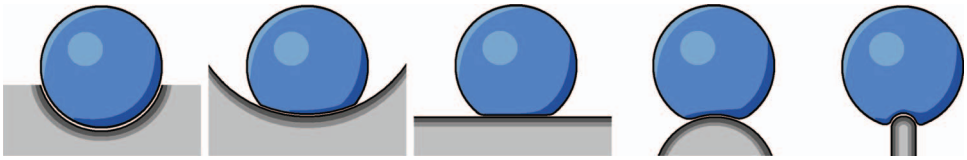

FIG. 1. A drop of radius R_0 impacts a rigid surface with radius of curvature R_2 (see Figure 2(b)). Several values of the curvature parameter $\mathcal{R} = 1 - R_0/R_2$ are shown: from left to right, $\mathcal{R} = 0$, $\mathcal{R} = 0.5$, $\mathcal{R} = 1$, $\mathcal{R} = 2$, and $\mathcal{R} \gg 1$.

surface tension. Considering the effects of the surrounding gas on the drop dynamics requires the inclusion of two more physical variables—the gas density ρ_g and gas viscosity μ_g—giving rise to two more nondimensional groups, ρ_g/ρ and $\mathbb{O}h_g = \mu_g (\sigma\rho R_0)^{-1/2}$. For the parameter range of interest, $\rho_g/\rho \ll 1$ and $\mathbb{O}h_g \ll \mathbb{O}h$, the influence of these two parameters is negligible. To incorporate the influence of substrate curvature, we consider the impacted solid to have a uniform radius of curvature R_2 and introduce the nondimensional group $\mathcal{R} = 1 - R_0/R_2$ (see Fig. 1). Defining the curvature of a concave substrate to be negative, we note that $\mathcal{R} = 1$ for a flat surface, $\mathcal{R} \to \infty$ for a sharp pin-shaped surface and $\mathcal{R} = 0$ for a surface whose curvature matches that of the drop.

Studies of liquid drop impact at small and moderate Weber numbers ($\mathbb{W}e < 30$) are scarce in comparison with their high Weber number counterparts. Foote[13] was the first to model numerically the dynamics of a nearly inviscid drop impacting a solid wall, his computations providing estimates for the contact time, contact area, and pressure distribution inside the drop. Gopinath and Koch[14] modeled the collision of two identical water drops at low Weber numbers by decomposing their deformation into spherical harmonic modes. In the limit $\ln(1/\mathbb{W}e) \gg 1$, they were able to use approximations of the behaviour of the Legendre polynomials $P_m(x)$ to show that the contact time increases logarithmically with decreasing $\mathbb{W}e$. The inherent symmetry of the collision of two *identical* drops means that it is in many ways equivalent to the rebound of a single drop from a flat rigid boundary and allows us to implement their results in the present paper.

Richard and Quéré[15] measured the coefficient of restitution C_R of small water drops (0.4 mm $\leq R_0 \leq$ 0.5 mm) bouncing on a super-hydrophobic surface for $0.02 \leq \mathbb{W}e \leq 2$. They reported C_R as large as 0.94, noting that it remains relatively constant above a critical impact velocity below which it sharply drops to zero, presumably because the contact angle hysteresis becomes important for sufficiently low Weber numbers. Richard *et al.*[16] measured the contact time T_C in the same configuration for $0.3 \leq \mathbb{W}e \leq 37$ and found it to be nearly independent of the Weber number in this range, with a slight increase at the lower end of the $\mathbb{W}e$ spectrum. Okumura *et al.*[17] measured the contact time in the same configuration for $0.003 \leq \mathbb{W}e \leq 1$ and two drop radii $R_0 = 0.4$ mm and $R_0 = 0.6$ mm, and noted an increase of T_C with decreasing $\mathbb{W}e$, which they attributed to the influence of gravity. They also presented a simple model for the drop dynamics, using a linear spring approximation to the reaction force obtained by approximating the drop distortion as a superposition of pure translation and vibration in the second fundamental harmonic mode.

Simple scaling suggests that the contact time scales as $T_C \approx A\left(\frac{\rho R_0^3}{\sigma}\right)^{1/2}$, as does the period of free oscillations of a drop.[18] The coefficient $A = A(\mathbb{B}o, \mathbb{W}e, \mathbb{O}h)$ is in general a function of the three nondimensional groups. However, when $\mathbb{W}e \gg \mathbb{B}o^2$, the effects of gravity can be neglected (Okumura *et al.*[17]); similarly, when $\mathbb{O}h \ll 1$, the effects of viscosity can be neglected. When these two conditions are met, we expect $A \approx A(\mathbb{W}e)$. Richard *et al.*[16] found experimentally that $A \approx 2.6$ for $1 < \mathbb{W}e < 30$, while the numerical models of Foote[13] and Gopinath and Koch[14] indicate that for $\mathbb{W}e < 1$, $A(\mathbb{W}e) \sim \ln\frac{1}{\mathbb{W}e}$. The linear spring model of Okumura *et al.*[17] predicts $A = 2.31$ independent of $\mathbb{W}e$, and thus must become invalid for sufficiently low $\mathbb{W}e$. We expect the coefficient of restitution C_R to depend most strongly on $\mathbb{O}h$, with $C_R \to 0$ as $\mathbb{O}h \to \infty$ and $C_R \to 1$ as $\mathbb{O}h \to 0$. Interestingly, for sufficiently high $\mathbb{W}e$, $\lim_{\mathbb{O}h\to 0} C_R \approx 0.91 < 1$, because part of the initial translational energy is transferred to oscillations of the drop surface, as demonstrated by Richard and Quéré.[15]

We here present a relatively simple model of non-wetting liquid drop impact valid in the limit of $\mathbb{W}e \ll 1$ that incorporates the influence of the curvature of the impacted surface. We approximate the drop shape at any instant by one from the quasi-static family of sessile shapes of a drop in a

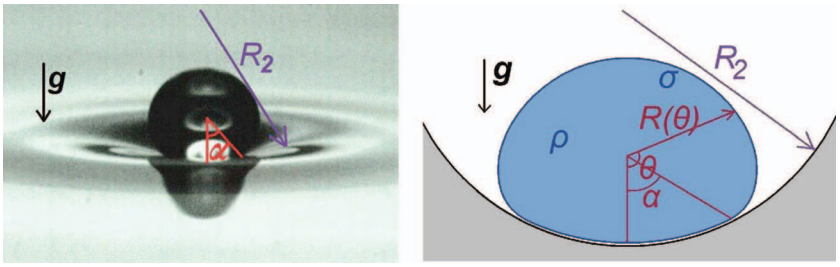

FIG. 2. Axisymmetric sessile drop of density ρ and surface tension σ resting on a surface with radius of curvature R_2. Without gravity, the drop would be spherical with radius R_0, under gravitational force $\boldsymbol{g}$ it deforms to a shape given by $R = R(\theta)$ in spherical coordinates. The drop shape conforms to that of the substrate over the area $0 \leq \theta \leq \alpha$.

homogeneous gravitational field. The precise shape is thus prescribed by the effective Bond number, which will be the single independent variable in our model. We proceed by finding the first order approximation to the static drop shape in Sec. II, which yields the change of the drop's surface and gravitational potential energies. In Sec. III, we find the spherical harmonic decomposition of the static shape, from which we derive the kinetic energy and viscous damping associated with a change of drop shape within the static shape family. We then form the Lagrangian of the system and derive the equation of motion. In Sec. IV, we analyze the asymptotic behaviour of contact time in the limit $\ln 1/\mathbb{W}e \gg 1$, both with and without the influence of gravity. We develop a simple numerical model to which we compare the predictions of the quasi-static model in cases where there are no existing data. We investigate the role of the substrate curvature on drop dynamics and show that to leading order the combined effects of curvature and impact speed can be described by a single nondimensional parameter.

II. THE SHAPE OF A STATIC DROP

The leading order deformation to a static drop caused by a weak uniform gravitational field was deduced by Chesters,[19] and subsequently considered by Smith and van De Ven,[20] Shanahan,[21] and Rienstra.[22] It will be briefly rederived here, in part to introduce the notation adopted in the paper. Consider a liquid drop with density ρ, surface tension σ, and undeformed radius R_0, that sits on a solid substrate with constant radius of curvature R_2. We set $R_2 > 0$ if the solid is concave (as in Fig. 2) and $R_2 < 0$ if it is convex. It will be useful to define the relative curvature parameter $\mathcal{R} = 1 - R_0/R_2$ (see Fig. 1). Under the influence of a weak gravitational acceleration g, the drop deforms to an axisymmetric shape given in spherical coordinates by

$$R(\theta) = R_0\,(1 + \epsilon f(\cos\theta))\,, \tag{1}$$

where $\epsilon \ll 1$. We place the center of our coordinate system at the droplet's center of mass, and align the vector $\theta = 0$ with gravity. We will assume a contact angle close to π, as our goal is to model the impact of water drops on super-hydrophobic surfaces, or drops which remain separated from the solid by a thin gas film. The drop shape conforms to that of the underlying solid in the region $0 \leq \theta \leq \alpha$. We write $\cos\alpha = 1 - \delta$, with δ being the *relative contact area*, specifically, the ratio of the contact area to its maximum possible value $2\pi R_0^2$, and assume $\alpha = O(\epsilon^{1/2})$, so that $\delta = O(\epsilon)$, as will be justified in what follows.

A. Drop energetics

The surface energy of the drop is given by

$$\begin{aligned}\mathcal{S}.\mathcal{E}. &= \sigma \int_0^{\pi} \left[2\pi R\sqrt{R^2 + R'^2}\sin\theta\right] d\theta \\ &= 2\pi\sigma R_0^2 \int_{-1}^{1} \left[1 + 2\epsilon f + \epsilon^2\left(f^2 + \frac{1}{2}f'^2(1-x^2)\right) + O\left(\epsilon^3\right)\right] dx,\end{aligned} \tag{2}$$

where $x = \cos\theta$. The potential energy of the drop is the height of its center of mass above a reference point, which we choose to be the intersection of the solid and the axis of symmetry of the system. Then, by definition of our coordinate system, we have, using (1)

$$\mathcal{P}.\mathcal{E}. = \frac{4}{3}\pi\rho g R_0^3\left[R(\alpha)\cos\alpha + \frac{(R(\alpha)\sin\alpha)^2}{2R_2}\right] = \frac{4}{3}\pi\rho g R_0^4\left[1 + \epsilon f(1-\delta) - \delta\mathcal{R} + O\left(\epsilon^2\right)\right]. \tag{3}$$

The volume of the droplet must remain constant under any deformation. Expressing the volume as an integral of $R(\theta)$ and integrating by parts once, we obtain $\frac{4}{3}\pi R_0^3 = \frac{2\pi}{3}\int_0^\pi R^3(\theta)\sin\theta d\theta$. Substituting again for $R(\theta)$ from (1) and using $x = \cos\theta$ yields

$$\int_{-1}^{1} f + \epsilon f^2 dx = O\left(\epsilon^2\right). \tag{4}$$

The condition that the center of mass is located at the origin is equivalent to $0 = \frac{\pi}{2}\int_0^\pi R^4(\theta)\sin\theta\cos\theta d\theta$. Once again, substituting from (1) yields

$$\int_{-1}^{1} f x dx = O\left(\epsilon\right). \tag{5}$$

In the contact region, the value of $f(x)$ is prescribed by the shape of the substrate

$$f(x) = \mathcal{R}\frac{1-x}{\epsilon} + \left(f(1-\delta) - \mathcal{R}\frac{\delta}{\epsilon}\right) \quad 1-\delta \le x \le 1. \tag{6}$$

Substituting for $\int_{-1}^{1} f dx$ from (4) into (2) gives

$$\mathcal{S}.\mathcal{E}. = 2\pi\sigma R_0^2\left[2 + \epsilon^2\int_{-1}^{1}\left(\frac{1}{2}f'^2(1-x^2) - f^2\right)dx + O\left(\epsilon^3\right)\right]. \tag{7}$$

Minimizing the total energy of the drop $\mathcal{E}_{TOT} = \mathcal{P}.\mathcal{E}. + \mathcal{S}.\mathcal{E}.$, subject to the constraints (4) and (5), leads to minimizing the functional $\int_{-1}^{1-\delta}\frac{1}{2}f'^2(1-x^2) - f^2 - \lambda_1 f - \lambda_2 f x\, \mathrm{d}x$, where λ_1, λ_2 are the Lagrange multipliers corresponding to the constraints (4) and (5), respectively. The Euler-Lagrange equation gives

$$\frac{d}{dx}\left[f'(1-x^2)\right] + 2f + \lambda_1 + \lambda_2 x = O\left(\epsilon\right). \tag{8}$$

The general solution of (8) (inhomogeneous Legendre's equation), which is well-behaved at $x = -1$, i.e., at $\theta = \pi$, is given by

$$f(x) = \frac{\lambda_2}{3}x\ln(1-x) + \frac{2-\lambda_1}{2} + cx. \tag{9}$$

We determine c and λ_1 from constraints (4) and (5). Absorbing λ_2 into ϵ finally gives

$$f(x) = \frac{x}{3}\ln\left(\frac{1-x}{2}\right) + \frac{1}{6} + \frac{4}{9}x + O\left(\epsilon\right), \tag{10}$$

which is equivalent to Eq. (12) in Shanahan.[21] Combining expressions (6) and (7), and substituting for $f(x)$ from (10) yields

$$\mathcal{S}.\mathcal{E}. = 2\pi\sigma R_0^2\left[2 - \frac{\epsilon^2}{9}\left(\ln\frac{\delta}{2} + \frac{11}{6}\right) + \frac{1}{2}\mathcal{R}^2\delta^2 + O\left(\epsilon^3\right)\right]. \tag{11}$$

Substituting for $f(x)$ from (10) into (3) and adding that to (11) yields an expression for the total energy

$$\frac{\mathcal{E}_{TOT}}{2\pi\sigma R_0^2} = 2 - \frac{\epsilon^2}{9}\left(\ln\frac{\delta}{2} + \frac{11}{6}\right) + \frac{1}{2}\mathcal{R}^2\delta^2 + \frac{2}{3}\mathbb{B}o\left[\epsilon\left(\frac{1}{3}\ln\frac{\delta}{2} + \frac{11}{18}\right) + \delta\mathcal{R}\right] + O\left(\epsilon^3\right). \tag{12}$$

Differentiating (12) with respect to ϵ gives $\epsilon = \mathbb{B}o$, differentiating with respect to δ then gives $\left(\delta\mathcal{R} - \frac{\mathbb{B}o}{3}\right)^2 = O\left(\mathbb{B}o^3\right)$, so

$$\delta = \frac{\mathbb{B}o}{3\mathcal{R}} + O\left(\mathbb{B}o^{3/2}\right). \tag{13}$$

We have thus determined the leading order change to the droplet shape due to gravity. The deformations are of order $\mathbb{B}o$ and so is the relative contact area δ, justifying the claim that $\alpha = O\left(\mathbb{B}o^{1/2}\right)$.

Using (13) we can now write the expressions for the surface and gravitational potential energy *increments*, that is, their change due to the drop deformation. It will be useful later on to include also the next order correction to these expressions, in order to obtain a better match for $\mathbb{B}o$ near 1. We have solved for the static shape numerically and, by subtracting the analytically derived first order dependence, were able to find that the second order correction is well approximated by $2\pi\sigma R_0^2 \frac{\mathbb{B}o^3}{18\mathcal{R}}$. Thus,

$$\begin{aligned}\frac{\Delta\mathcal{S}.\mathcal{E}.}{2\pi\sigma R_0^2} &\approx +\frac{1}{9}\mathbb{B}o^2\left[\ln\frac{6\mathcal{R}}{\mathbb{B}o} - \frac{4}{3} + \frac{\mathbb{B}o}{2\mathcal{R}}\right],\\ \frac{\Delta\mathcal{P}.\mathcal{E}.}{2\pi\sigma R_0^2} &\approx -\frac{2}{9}\mathbb{B}o^2\left[\ln\frac{6\mathcal{R}}{\mathbb{B}o} - \frac{5}{6} + \frac{3\mathbb{B}o}{8\mathcal{R}}\right].\end{aligned} \tag{14}$$

Expression (14) is in accord with the result of Morse and Witten,[23] who found that the surface energy of a drop subject to a point force f increases by an amount proportional to $f^2\ln(1/f)$.

B. Spherical harmonic decomposition

In order to compute the kinetic energy of the quasi-static drop in Sec. III, we will need the spherical harmonic decomposition of the static axisymmetric profile:

$$R(\theta) = R_0\left(1 + \mathbb{B}o f(\cos\theta)\right) = R_0\left(1 + \mathbb{B}o\sum_{n=2}^{\infty} b_n P_n(\cos\theta)\right), \tag{15}$$

where P_n is the nth Legendre polynomial. The sum begins with $n = 2$ because $b_0 = 0$ from volume conservation (4) and $b_1 = 0$ from (5). A static drop minimizes the sum of its surface energy and gravitational potential energy.

In order to obtain the surface energy in terms of the spherical harmonic components, we substitute $f(x) = \sum_{n=2}^{\infty} b_n P_n(\cos x)$ from (15) into (7), which yields

$$\frac{\mathcal{S}.\mathcal{E}.}{2\pi\sigma R_0^2} = 2 + \mathbb{B}o^2\sum_{m,n=2}^{\infty} b_m b_n \int_{-1}^{1}\frac{1}{2}(1-x^2)P_m' P_n' - P_m P_n dx + O\left(\mathbb{B}o^3\right). \tag{16}$$

Orthogonality of the Legendre polynomials and integration by parts yields

$$\mathcal{S}.\mathcal{E}. = 4\pi\sigma R_0^2 + 2\pi\sigma R_0^2\mathbb{B}o^2\sum_{m=2}^{\infty}\frac{(m-1)(m+2)}{2m+1}b_m^2 + O\left(\mathbb{B}o^3\right). \tag{17}$$

Obtaining the gravitational potential energy is less straightforward. It might be tempting to simply use (3) and write $\mathcal{P}.\mathcal{E}. = \frac{4}{3}\pi\rho g R_0^4\left[1 + \mathbb{B}o\sum_{m=2}^{\infty} b_m P_m(1-\delta) - \delta\mathcal{R}\right]$ with δ given by (13). This is equivalent to a drop resting on a circular wire of radius $R_0\sqrt{2\delta}$. An alternative choice would be to set $\delta = 0$ in the previous expression, which is equivalent to constraining the drop at just one point. Both approaches are unsatisfactory, especially the latter, as indicated in Fig. 3. Although they both give correct values of b_m in the limit of $\delta \to 0$ (i.e., $\mathbb{B}o \to 0$), we want a good approximation to the next order corrections, which will be used in calculating the kinetic energy and also in the reference numerical simulation. To that end, we must somehow constrain the drop over the whole

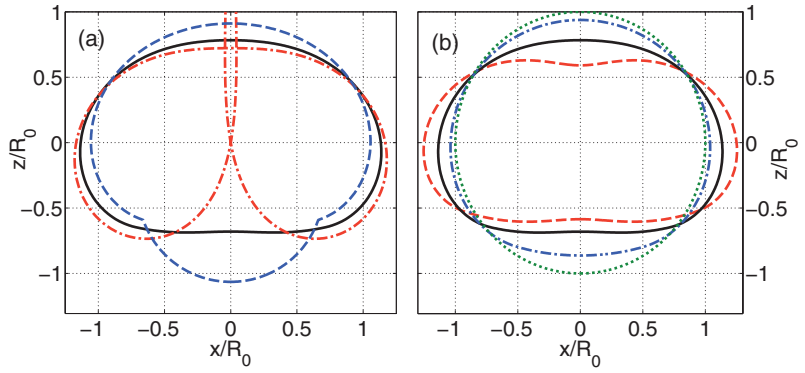

FIG. 3. (a) The static profiles of a liquid drop with $\mathbb{B}o = 1$ on a flat surface. The three profiles are the sum of the first 50 spherical harmonic modes obtained by minimizing the surface and gravitational potential energy of a drop constrained in different ways, by averaging the reaction force over: the contact area (Eq. (19)) (solid line), the contact area rim (dashed line), and the center of the contact area (dashed-dotted line). We see that even for an $O(1)$ Bond number, the averaging method provides a good approximation to the actual drop shape, which has a perfectly flat base. (b) The static profile of a drop obtained from the first 50 spherical harmonics using the averaging method (20) for several values of $\mathbb{B}o$: $\mathbb{B}o = 0$ (dotted line), $\mathbb{B}o = 0.5$ (dashed-dotted line), $\mathbb{B}o = 1$ (solid line) and $\mathbb{B}o = 1.5$ (dashed line).

contact area. A simple way to do that is to use the average over that region:

$$\mathcal{P}.\mathcal{E}. = \frac{4}{3}\pi\rho g R_0^4 \left[1 + \frac{1}{\delta}\int_{1-\delta}^{1} \mathbb{B}o \sum_{m=2}^{\infty} b_m P_m(x) - (1-x)\mathcal{R}\mathrm{d}x\right]. \tag{18}$$

Since $\int_{1-\delta}^{1} P_m(x)\mathrm{d}x = \frac{2\delta-\delta^2}{m(m+1)} P_m'(1-\delta)$, (18) can be written

$$\mathcal{P}.\mathcal{E}. \approx \frac{4}{3}\pi\rho g R_0^4 \left[1 + 2\mathbb{B}o \sum_{m=2}^{\infty} b_m \frac{P_m'(1-\delta)}{m(m+1)}\right]. \tag{19}$$

Minimizing the sum of (17) and (19) with respect to each b_m immediately yields

$$b_m \approx -\frac{2}{3}\frac{(2m+1)P_m'(1-\delta)}{(m-1)m(m+1)(m+2)} \quad \text{with } \delta = \frac{\mathbb{B}o}{3\mathcal{R}}. \tag{20}$$

As $\mathbb{B}o \to 0$, $b_m \to -\frac{1}{3}\frac{2m+1}{(m-1)(m+2)}$, the result obtained from the point constraint for all $\mathbb{B}o$. Including more modes obtained by the point constraint method therefore leads to a shape that diverges logarithmically at $x = 1$ (see Fig. 3(a)). This divergence is avoided by our averaging method (20), which produces a good representation of the contact area even for large values of $\mathbb{B}o$. In Fig. 3(a), it is evident that the form obtained by our averaging method is nearly flat over the contact area, instead of bulging outwards as does the form obtained by the rim constraint method, or curving inwards as does the form obtained by the point constraint method. In Fig. 3(b), we show the static drop shape obtained by the averaging method for several values of $\mathbb{B}o$. Once again, the curves are close to flat throughout the contact area for all values of $\mathbb{B}o$ considered.

III. QUASI-STATIC DROPLET

We now assume that the drop shape is given by

$$R(\theta, t) = R_0\left(1 + B(t) f(B, \cos\theta)\right) = R_0\left(1 + B(t)\sum_{n=1}^{\infty} b_n(B)\, P_n(\cos\theta)\right), \tag{21}$$

that is, it corresponds to that of a static drop with instantaneous effective Bond number $\mathbb{B}o_{eff} = B(t)$. The surface and gravitational potential energy of the drop are obtained by simply replacing $\mathbb{B}o$ by $B(t)$ in (14). We want to calculate the kinetic energy and rate of viscous dissipation corresponding to

this motion in the center-of-mass frame of reference. Let us first consider the limit of small viscosity, which is most accessible analytically.

A. $\mathbb{O}h \ll 1$: Low viscosity drops

When the ratio of the viscous to surface tension forces, as prescribed by the Ohnesorge number $\mathbb{O}h = \mu\,(\rho\sigma R_0)^{-1/2}$, is sufficiently small, we can approximate the flow inside the drop by a potential flow. Axisymmetric solutions of the Laplace equation $\nabla^2\phi = 0$ in spherical coordinates for the velocity potential ϕ, which are continuous at the origin, are of the form $r^n P_n(\cos\theta)$. We can thus write

$$\phi(r,\theta,t) = \sum_{n=1}^{\infty} R_0^2 \left(\frac{r}{R_0}\right)^n \dot{\Phi}_n(t) P_n(\cos\theta). \tag{22}$$

The radial component of velocity is then given by

$$\boldsymbol{u}_r(r,\theta,t) = \boldsymbol{e}_r \frac{\partial\phi}{\partial r} = R_0 \boldsymbol{e}_r \sum_{n=1}^{\infty} n \left(\frac{r}{R_0}\right)^{n-1} \dot{\Phi}_n(t) P_n(\cos\theta)\,. \tag{23}$$

Application of boundary conditions at the surface yields

$$u_r(R_0,\theta,t) = \frac{\partial R(\theta,t)}{\partial t} = R_0 \dot{B}(t) \sum_{n=1}^{\infty} b_n P_n(\cos\theta), \tag{24}$$

using (22) and ignoring the terms $B(t)\dot{b}_n$ which are of order B^2. Therefore, $\Phi_n(t) = B(t)b_n/n$. The kinetic energy of the drop is given by

$$\begin{aligned}\mathcal{K}.\mathcal{E}._0 &= \frac{1}{2}\rho \int_V \nabla\phi\cdot\nabla\phi dV = \frac{1}{2}\rho \int_V \nabla\cdot(\phi\nabla\phi)\,\mathrm{d}V = \frac{1}{2}\rho \int_S \phi \boldsymbol{u}_r \mathrm{d}S = \\ &= \pi R_0^5 \rho \int_0^{\pi} \left(\sum_m \dot{B} b_m P_m \frac{1}{m}\right)\left(\sum_n \dot{B} b_n P_n\right) \sin\theta \mathrm{d}\theta = \pi\rho R_0^5 \dot{B}^2(t) \sum_{m=2}^{\infty} \frac{2b_m^2}{m(2m+1)},\end{aligned} \tag{25}$$

where we have used $\nabla^2\phi = 0$ and the orthogonality of the Legendre polynomials. Using the rotational symmetry, the viscous dissipation in the drop can be written as

$$\mathcal{D} = 2\mu \int_V \left(\frac{\partial u_r}{\partial r}\right)^2 + \left(\frac{1}{r}\frac{\partial u_\theta}{\partial\theta} + \frac{u_r}{r}\right)^2 + \left(\frac{u_r}{r}\right)^2 + \frac{1}{2}\left(r\frac{\partial}{\partial r}\frac{u_\theta}{r} + \frac{1}{r}\frac{\partial u_r}{\partial\theta}\right)^2 \mathrm{d}V. \tag{26}$$

For small $\mathbb{O}h$, we can substitute for $\boldsymbol{u} = \nabla\phi$ from (22) into the general formula above, and so derive the expression

$$\mathcal{D}_0 = 8\pi\mu R_0^3 \dot{B}^2(t) \sum_{m=2}^{\infty} \frac{m-1}{m} b_m^2. \tag{27}$$

Having computed the coefficients b_m we can now derive closed-form expressions for the kinetic energy and energy dissipation rate. In the $\mathbb{B}o \to 0$ limit, we have $b_m = -\frac{1}{3}\frac{2m+1}{(m-1)(m+2)}$, which implies

$$\mathcal{K}.\mathcal{E}._0 = \frac{2}{9}\pi\rho R_0^5 \dot{B}^2 \sum_{m=2}^{\infty} \frac{2m+1}{m(m-1)^2(m+2)^2} = \frac{2}{9}\pi\rho R_0^5 \dot{B}^2 C_{K0} \quad \mathbb{B}o \ll 1, \tag{28}$$

where $C_{K0} = \frac{\pi^2}{12} - \frac{17}{27} = 0.19284\ldots$, and the energy dissipation rate is

$$\mathcal{D}_0 = \frac{8}{9}\pi\mu R_0^3 \dot{B}^2 \sum_{m=2}^{\infty} \frac{(2m+1)^2}{m(m+2)^2(m-1)} = \frac{8}{9}\pi\mu R_0^3 \dot{B}^2 C_{D0} \quad \mathbb{B}o \ll 1, \tag{29}$$

where $C_{D0} = \frac{\pi^2}{4} - \frac{5}{12} = 2.0507\ldots$.

For a finite B, we substitute (20) into (25) and (27). It is found that the formulae (28) and (29) overestimate the kinetic energy and dissipation rate for $B = O(1)$. Although no closed-form expressions could be found for these two quantities at finite B, a reasonable approximation is given by

$$\mathcal{K}.\mathcal{E}._0(B) \approx \frac{2}{9}\pi\rho R_0^5 \dot{B}^2 C_{K0}\,(1 - M(B)) \quad \text{and } \mathcal{D}_0(B) \approx \frac{8}{9}\pi\mu R_0^3 \dot{B}^2 C_{D0}\left(1 - \sqrt{M(B)}\right), \tag{30}$$

where $M(B) = \frac{8B}{27\mathcal{R}} \ln \frac{9\mathcal{R}}{B}$.

B. Arbitrary $\mathbb{O}h$

For arbitrary $\mathbb{O}h$, the potential flow approximation ceases to be valid and one has to use a more general method to derive the kinetic energy and viscous dissipation. For small B, the spherical harmonic modes are still uncoupled, but now we have

$$\mathcal{K}.\mathcal{E}. = \pi\rho R_0^5 \dot{B}^2(t) \sum_{m=2}^{\infty} A_m(\mathbb{O}h_m) \frac{2b_m^2}{m(2m+1)} \quad \mathcal{D} = 8\pi\mu R_0^3 \dot{B}^2(t) \sum_{m=2}^{\infty} D_m(\mathbb{O}h_m) \frac{m}{2m+1} b_m^2. \tag{31}$$

The scaled Ohnesorge number $\mathbb{O}h_m \equiv \mathbb{O}h\sqrt{m}$ is introduced for the sake of convenience. The coefficients A_m and D_m are such that the roots of the equation

$$A_m b^2 - 2a D_m b + 1 = 0, \quad \text{where } a = \frac{\mathbb{O}h}{\sqrt{m(m-1)(m+2)}}, \tag{32}$$

are the two roots with the largest real part of the transendental equation

$$b^2 - 2a(m-1)\frac{[(2m+1) - 2m(m+2)W(b/a)]}{1 - 2W(b/a)} b + 1 = 0, \quad \text{where } W(x) = \frac{J_{m+3/2}(\sqrt{x})}{\sqrt{x} J_{m+1/2}(\sqrt{x})}. \tag{33}$$

Here, $J_k(x)$ is the Bessel function of the first kind of order k and a is defined in (32). For the derivation of (33), see Chandrasekhar[24] or Miller and Scriven.[25] The dependence of A_m and D_m on $\mathbb{O}h_m$ is shown on Fig. 4. From the properties of the Bessel functions, it follows that $W(x) \to \frac{1}{2m+3}$ as $x \to 0$ and $W(x) \to 0$ as $x \to \infty$. This allows one to approximate (32) in the limits of $\mathbb{O}h \to 0$ and $\mathbb{O}h \to \infty$.[25] For low viscosity ($\mathbb{O}h_m < 0.03$), $A_m \to 1$ (as derived in Sec. III A) and $D_m \to \frac{(2m+1)(m-1)}{m^2}$. For high viscosity ($\mathbb{O}h_m > 1$), $D_m \to \frac{(m-1)(2m^2+4m+3)}{m^2(2m+1)}$ and the kinetic energy term is negligible relative to the

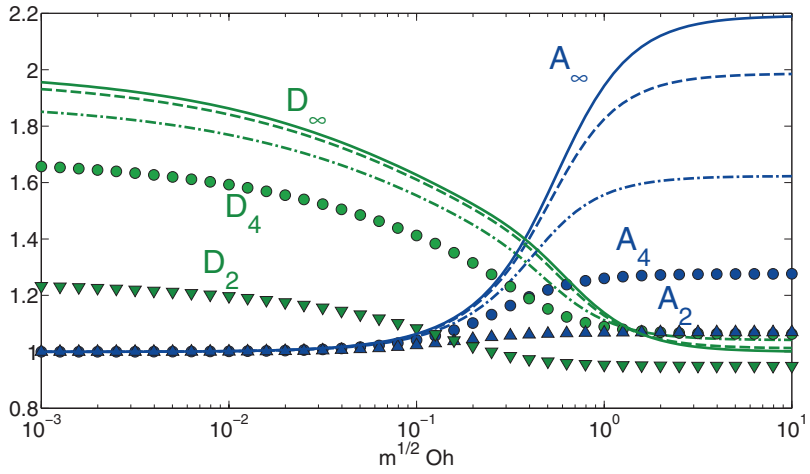

FIG. 4. The dependence of the coefficients A_m and D_m from Eq. (31) on the scaled Ohnesorge number $\mathbb{O}h_m = m^{1/2}\mathbb{O}h$. Curves for $m = 2$, 4, 10, 40 (triangles, circles, dashed-dotted, and dashed lines, respectively) are shown, together with the limiting curves for $m \to \infty$ (solid lines) corresponding to planar surface capillary waves.

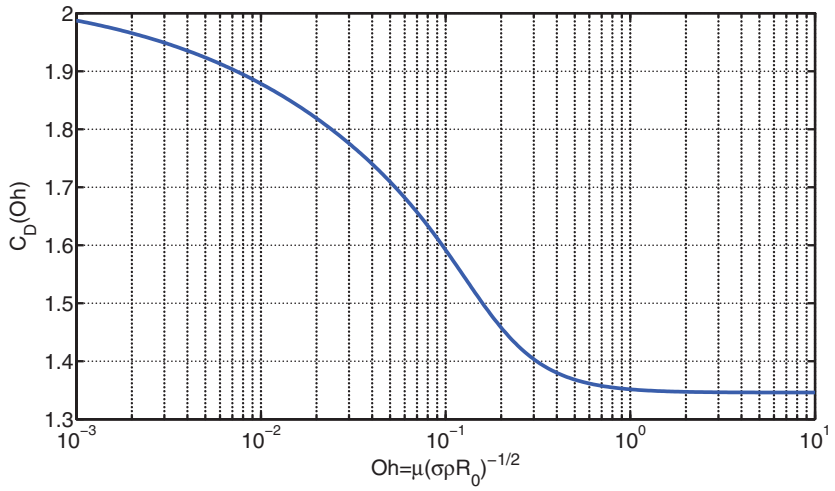

FIG. 5. The dependence of the dissipation coefficient C_D in Eq. (34) on the Ohnesorge number $\mathbb{O}h$.

surface energy term and so can be discarded. As $m \to \infty$, the values of $A_m(\mathbb{O}h_m)$ and $D_m(\mathbb{O}h_m)$ approach limiting values, denoted $A_\infty(\mathbb{O}h_m)$, $D_\infty(\mathbb{O}h_m)$, which coincide with the values obtained for small surface capillary waves on a planar surface. Note that $D_\infty(0) = 2$, while $D_\infty(\infty) = 1$ (see Fig. 4).

As in Sec. III A, we substitute for b_m from (20) into (31) to find that

$$\mathcal{K}.\mathcal{E}.(B, \mathbb{O}h) \approx \frac{2}{9}\pi\rho R_0^5 \dot{B}^2 C_K(\mathbb{O}h)(1-M), \quad \mathcal{D}(B, \mathbb{O}h) \approx \frac{8}{9}\pi\mu R_0^3 \dot{B}^2 C_D(\mathbb{O}h)\left(1-\sqrt{M}\right), \tag{34}$$

where $M(B) = \frac{8B}{27\mathcal{R}} \ln \frac{9\mathcal{R}}{B}$.

C_K is a monotonically increasing function of $\mathbb{O}h$, but since $C_K(0) = C_{K0} = 0.192$ while $C_K(\infty) = 0.212$, we can approximate the kinetic term by C_{K0} henceforth while incurring no more than a 5% error. On the other hand, C_D is a monotonically decreasing function of $\mathbb{O}h$ (see Fig. 5) with $C_D(0) = \frac{\pi^2}{4} - \frac{5}{12} = 2.051$ and $C_D(\infty) = \frac{\pi^2}{12} + \frac{19}{36} = 1.350$, so for problems with $0.01 \le \mathbb{O}h \le 1$ one cannot use either of the limiting values without sacrificing accuracy. Prosperetti[26,27] treats this complication in greater detail.

C. Equation of motion

Having derived the surface, kinetic and gravitational potential energies of the drop, as well as the viscous dissipation inside it, we can now construct the Lagrangian $\mathfrak{L} = \mathcal{K}.\mathcal{E}. - \Delta\mathcal{S}.\mathcal{E}. - \Delta\mathcal{P}.\mathcal{E}.$ We switch to a coordinate system fixed to the impacted surface, and assume that it is stationary. The kinetic energy must thus also include a contribution from movement of the drop's center of mass. We define $R_0 b_1$ to be the vertical displacement of the center of mass relative to where it would be if the drop remained spherical. Its dependence on B can be obtained from (14) since $\Delta\mathcal{P}.\mathcal{E}. = -\frac{4}{3}\pi\rho g R_0^4 b_1$:

$$b_1 = \frac{B}{3}\left[\ln\frac{6\mathcal{R}}{B} - \frac{5}{6} + \frac{3B}{8\mathcal{R}}\right]. \tag{35}$$

Then, as $\frac{d}{dt}b_1 = b_1'(B)\dot{B}$, the Lagrangian is

$$\mathfrak{L} = \pi\rho R_0^5\left[\frac{2}{3}\left(b_1'\dot{B}\right)^2 + \frac{2}{9}C_{K0}(1-M(B))\dot{B}^2\right] - \Delta S.E.(B) + \frac{4}{3}\pi\rho g R_0^4 b_1. \tag{36}$$

We obtain the drop's equation of motion using the Euler-Lagrange equation with dissipation[28]

$$\frac{d}{dt}\left[\frac{\partial \mathfrak{L}}{\partial \dot{B}}\right] + \frac{1}{2}\frac{\partial \mathcal{D}}{\partial \dot{B}} = \frac{\partial \mathfrak{L}}{\partial B}. \tag{37}$$

After nondimensionalizing the time with $\tau = t\left(\sigma/\rho R_0^3\right)^{1/2}$, we deduce

$$\left[b_1'^2 + \frac{1-M}{3}C_{K0}\right]\frac{d^2B}{d\tau^2} + \left[b_1' b_1'' - \frac{M'}{6}C_{K0}\right]\left(\frac{dB}{d\tau}\right)^2 + 2\mathbb{O}h\frac{1-\sqrt{M}}{3}C_D\frac{dB}{d\tau} + b_1'(B-\mathbb{B}o) = 0, \tag{38}$$

where dashes indicate derivatives with respect to B. $M(B)$ is given by (34), $C_{K0} = \frac{\pi^2}{12} - \frac{17}{27} = 0.1928$, and $C_D(\mathbb{O}h)$ is shown on Fig. 5. We have used the relation $\frac{d\Delta S.E.}{dB} = -\frac{4}{3}\pi\sigma R_0^2 b_1' B$, which follows from the fact that the stationary droplet shape minimizes the sum of potential and surface energy. Differentiating (35), we obtain

$$b_1'(B) = \frac{1}{3}\left[\ln\frac{6\mathcal{R}}{B} - \frac{11}{6} + \frac{3B}{4\mathcal{R}}\right] \quad \text{and} \quad b_1''(B) = \frac{3B/4\mathcal{R} - 1}{3B}. \tag{39}$$

When $\ln(6\mathcal{R}/B) \gg 1$, (38) can be greatly simplified by neglecting higher order terms in B, giving

$$\left[\ln\frac{6\mathcal{R}}{B} - \frac{11}{6}\right]B_{\tau\tau} - B_\tau^2/B + 3(B-\mathbb{B}o) = 0. \tag{40}$$

Equation (38), or its small $\mathbb{B}o$ approximation (40), is our final equation describing the dynamics of a quasi-static droplet. In terms of simplicity and speed of numerical solution, it is surpassed only by the linear spring model of Okumura *et al.* In contrast to the latter model however, it compares favourably even with extensive numerical simulations and experiments, as will be shown in what follows.

IV. RESULTS

In this section, we compare the results obtained with our quasi-static model with previous models and, most decisively, experimental results reported in the literature. In order to evaluate the accuracy of the model for parameters not found in the literature (e.g., different values of $\mathcal{R}$), we have also created a numerical model by considering the spherical harmonic decomposition of the drop (15). The Lagrangian constructed from the surface energy (17), potential energy (19), and kinetic energy (31), together with the constraint

$$\int_{1-\delta}^{1} \sum b_m P_m(x) - (1-x)\mathcal{R}\,\mathrm{d}x = 0, \tag{41}$$

allows one to obtain the equation of motion for each of the modes:

$$A_m b_{m\tau\tau} + 2m^2\mathbb{O}h D_m b_{m\tau} + m(m-1)(m+2)b_m + \delta_{1m}\mathbb{B}o + \lambda\frac{2m+1}{m+1}P_m'(1-\delta) = 0, \tag{42}$$

where $\tau = t\left(\sigma/\rho R_0^3\right)^{1/2}$ and δ_{ij} is the Kronecker delta function. δ is defined as the largest solution of $f(1-x) = \mathcal{R}x$ (the length over which the drop surface conforms to that of the substrate), where $f(x) = \sum_{m=1}^{M} b_m P_m(x)$. λ is the Lagrange multiplier corresponding to the constraint (41) and its value is determined at each step so that the value of the left-hand side of (41) remains constant except possibly for discrete jumps when δ changes discontinuously. We used $M = 150$ modes in our calculations, but as few as 20 modes are sufficient to achieve good accuracy (relative to the full $M = 150$ simulations) within the range of Weber and Bond numbers examined.

A. Contact time of an impacting drop

Our quasi-static model provides a simple way of treating the vibrations and impact of small drops on a rigid surface for small Weber numbers. Drops impacting with speed V can be modeled

by the Eq. (38) with initial conditions $B(0) = \epsilon$, $B_\tau(0) = \mathbb{W}e^{1/2}/b_1'(\epsilon)$ with $\epsilon \to 0$. The contact time of impacting drops has been studied experimentally by Richard *et al.*,[15] Okumura *et al.*,[17] and numerically by Foote[13] and Gopinath and Koch.[14] Comparing the contact time obtained by solving (38) numerically with their results will allow us to determine the range of validity of our quasi-static model.

Note that from (40), we can obtain T_C in the low speed limit $\mathbb{W}e \to 0$, where we expect $B = O\left(\mathbb{W}e^{1/2}\right)$ from conservation of energy. For $\mathbb{B}o \ll \mathbb{W}e^{1/2}$, the influence of gravity on the droplet dynamics can be neglected. By assuming $B(\tau) = A\sin\omega\tau$ with $A \ll 1$ and approximating $\ln(\mathcal{R}/B(t)) \approx \ln(\mathcal{R}/A)$, one can reduce (40) to $\omega^2 \ln(\mathcal{R}/A) \approx 3$, thus $\tau_C = \frac{\pi}{\omega} \approx \pi\sqrt{\frac{\ln(\mathcal{R}/A)}{3}}$. From the initial condition $A\omega = B_\tau(0) \approx 3\mathbb{W}e^{1/2}\ln^{-1}(\mathcal{R}/A)$, it follows that $A\ln^{1/2}(\mathcal{R}/A) \approx \sqrt{3}\mathbb{W}e^{1/2}$ and so $\tau_C \approx \frac{\pi}{\sqrt{3}}\left[\ln\frac{\mathcal{R}}{\mathbb{W}e^{1/2}} + \ln\ln^{1/2}\frac{\mathcal{R}}{\mathbb{W}e^{1/2}} + \gamma\right]^{1/2}$. Analysis of numerical solutions to (40) allows us to determine γ and so deduce

$$T_C = \pi\sqrt{\frac{\rho R_0^3}{3\sigma}}\left[\ln\frac{\mathcal{R}}{\mathbb{W}e^{1/2}} + \ln\ln^{1/2}\frac{\mathcal{R}}{\mathbb{W}e^{1/2}} + 0.55\right]^{1/2} + O\left(\ln^{-1}\mathbb{W}e^{-1/2}\right) \quad \text{for } \mathbb{B}o \ll \mathbb{W}e^{1/2}. \tag{43}$$

The expression (43) represents an improvement on the first analytic expression for the contact time, formula (2.19) from Gopinath and Koch,[14] which states $T_C = \pi\sqrt{\frac{\rho R_0^3}{3\sigma}}\left[\ln\mathbb{W}e^{-1/2} + O\left(\ln\ln^{1/2}\mathbb{W}e^{-1/2}\right)\right]^{1/2}$ for the case of a flat impactor $\mathcal{R} = 1$. (43) implies that the nondimensional contact time increases without bound as the Weber number approaches zero; however, in reality the effects of viscosity and other body forces will alter this result for sufficiently small Weber numbers.

When $1 \gg \mathbb{B}o \geq \mathbb{W}e^{1/2}$, we assume that the drop's center of mass will oscillate around its equilibrium position: $B(\tau) = \mathbb{B}o\,(1 + A\cos\omega\tau)$. The value of the amplitude A is determined from the conservation of energy. The kinetic energy associated with the internal circulation is negligible relative to its translational kinetic energy, as can be seen from (38), their ratio being $3C_{K0}/\ln^2\frac{6\mathcal{R}}{B} \ll 1$. Thus, the initial kinetic energy of the drop $\frac{2}{3}\pi\rho R_0^3 V^2$ must equal the sum of surface and gravitational potential energy at the instant of maximal drop deformation, i.e., when $B = \mathbb{B}o(1 + A)$. Substituting for B into (14) yields $A^2 = 1 + 3\mathbb{W}e/\left(\mathbb{B}o^2\ln\frac{\mathcal{R}}{\mathbb{B}o}\right)$, provided $\ln\frac{\mathcal{R}}{\mathbb{B}o} \gg 1$. The contact time equals the difference between the two times when $0 = B(\tau) = \mathbb{B}o\,(1 + A\cos\omega\tau)$, so $\tau_c = \frac{2}{\omega}\left(\pi - \cos^{-1}A^{-1}\right)$. In order to obtain ω, we calculate the frequency of small oscillations around the equilibrium drop shape. Substituting $B(\tau) = \mathbb{B}o\left(1 + \epsilon e^{i\omega\tau}\right)$ into (40) with $\epsilon \ll 1$, gives $\omega \approx \sqrt{\frac{1}{3}\ln(\mathcal{R}/\mathbb{B}o) + C_K\ln^{-1}(\mathcal{R}/\mathbb{B}o)}$. Therefore,

$$T_C \approx 2\left[\frac{\rho R_0^3}{\sigma}\left(\frac{\ln\frac{\mathcal{R}}{\mathbb{B}o}}{3} + \frac{C_K}{\ln\frac{\mathcal{R}}{\mathbb{B}o}}\right)\right]^{1/2}\left[\pi - \arccos\left(1 + \frac{3\mathbb{W}e}{\mathbb{B}o^2\ln\frac{\mathcal{R}}{\mathbb{B}o}}\right)^{-1/2}\right] \quad \text{for} \quad \mathbb{B}o \geq \mathbb{W}e^{1/2}. \tag{44}$$

The results are shown in Figures 6–8. In Fig. 6, we see that the numerical model (42), the quasi-static models (38) and (40), and the predictions of Gopinath and Koch[14] all converge for small $\mathbb{W}e$, as expected. Our numerical model is also in good agreement with the numerical results of Foote,[13] the difference for $\mathbb{W}e \sim 1$ being due to the fact that the drop becomes elongated upon detachment from the surface, thus prolonging the contact time. This effect was included in Foote's model, but to capture it within the quasi-static framework, one would need to decouple the contact area size from the overall drop deformation and solve for the static shape in negative gravity. While such decoupling would represent an interesting extension of the quasi-static model and presumably would allow one to better capture the dynamics for $\mathbb{W}e = O(1)$, as our primary focus was the small $\mathbb{W}e$ limit, this direction was not pursued. Note also that in the numerical simulation using (42), we set the contact time to be the time necessary for b_1 to pass zero, i.e., for the center of mass to return to its initial position before the contact. This alternative definition of contact time, while making no difference within the quasi-static framework, was made to eliminate the effects of the oscillations

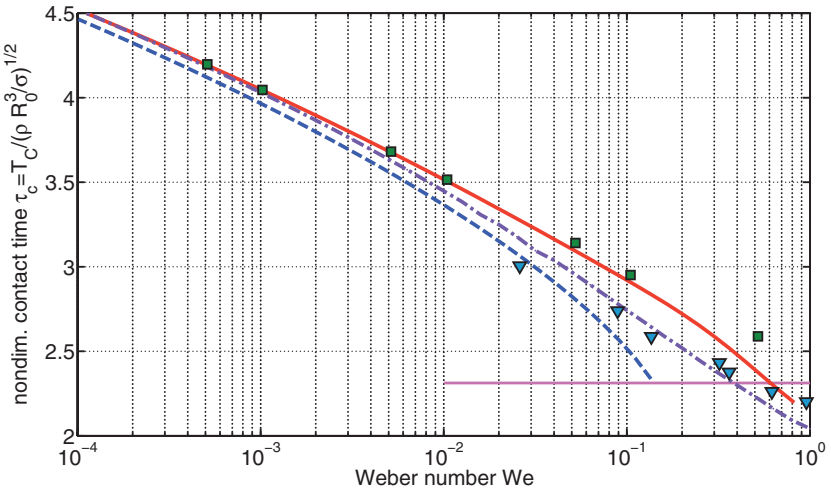

FIG. 6. Comparison of the nondimensional contact time $\tau_c = T_C/\left(\rho R_0^3/\sigma\right)^{1/2}$ as a function of the Weber number $\mathbb{W}e = \rho R_0^2 V_{in}^2/\sigma$ for $\mathbb{O}h = \mu/(\rho\sigma R_0)^{1/2} = 0.005$ and $\mathbb{B}o = \rho g R_0^2/\sigma = 0$, obtained with our quasi-static model (38) (solid line), the simplified model (40) (dashed line), and numerical simulation of the first 250 spherical harmonic modes (42) (dashed-dotted line). The predictions of Gopinath and Koch[14] (■), Foote[13] (▼), and Okumura[17] (horizontal line) are included for the sake of comparison.

of higher spherical modes on the actual contact time (inevitable for $\mathbb{O}h \to 0$) and thus show the general trends more clearly.

We can see from Fig. 6 that the full quasi-static model is within 12% of the other results for the entire range of Weber numbers studied, while the simplified quasi-static model (40) is within 10% for $\mathbb{W}e \lesssim 0.1$. The spring model of Okumura *et al.*[17] predicts $\tau_C = \pi\sqrt{13/24} = 2.312$, which we see is only approximately valid for $0.2 < \mathbb{W}e \lesssim 1$. For smaller Weber numbers, one needs to include more spherical harmonic modes. In fact, one finds that modeling the first N spherical harmonic modes together with the constraint $\sum_{n=1}^{N} b_n = 0$ (drop pinned at one point) gives $\tau_c \approx \pi\sqrt{\frac{2}{3}\ln N}$.

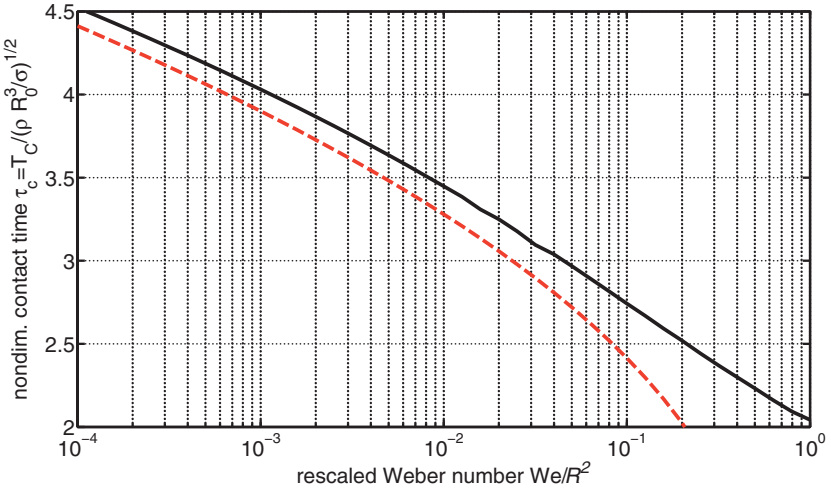

FIG. 7. The dependence of the nondimensional contact time $\tau_c = T_C\left(\sigma/\rho R_0^3\right)^{1/2}$ on the rescaled Weber number $\mathbb{W}e/\mathcal{R}^2 = \rho R_0 V_{in}^2/\sigma(1 - R_0/R_2)^2$. Results of the numerical model (42) for several values ($0.1 \le \mathcal{R} \le 10$) of the curvature parameter $\mathcal{R} = 1 - R_0/R_2$ follow a single curve (solid line). The analytic expression (43) (dashed line) is shown for the sake of comparison.

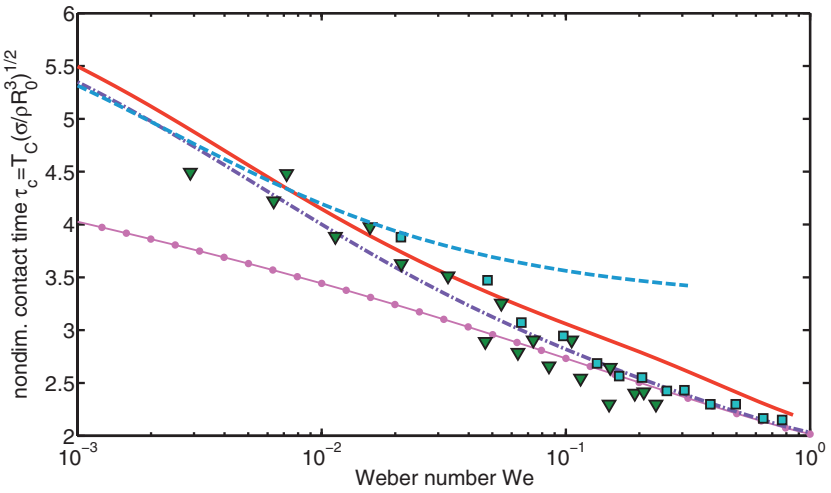

FIG. 8. The effects of gravity on the nondimensional contact time $\tau_C = T_C\sqrt{\frac{\sigma}{\rho R_0^3}}$ as a function of the Weber number $\mathbb{W}e = \rho R_0 V_{in}^2/\sigma$. The results of the numerical model (42) (dashed-dotted line), quasi-static model (38) (solid line), and the analytical expression (44) (dashed line), all for $\mathbb{B}o = 0.05$ are plotted, together with the experimental results of Okumura *et al.*, for $\mathbb{B}o = 0.02$ (▼) and $\mathbb{B}o = 0.05$ (■). For reference, the result of the numerical model (42) for $\mathbb{B}o = 0$ (i.e., no gravity) is also shown (●).

By comparison with formula (43), we see that one should include at least $N \approx \frac{\sqrt{\mathcal{R}}}{\mathbb{W}e^{1/4}} \ln^{1/4} \frac{\mathcal{R}}{\mathbb{W}e^{1/2}}$ modes for reliable results.

The analytic expression (43) suggests that one should use the rescaled Weber number $\mathbb{W}e/\mathcal{R}^2$ to incorporate the effects of curvature and Weber number into a single nondimensional group; indeed, the numerical results for different $\mathcal{R}$ then collapse onto a single curve (see Fig. 7). It can be shown that this collapse follows from the nature of the linearized boundary conditions and equations employed, which are valid approximations provided the contact area, that is, the size of the region over which the drop's shape conforms to that of the substrate, remains small relative to the total drop area. This relative contact area is proportional to δ, which we know from (13) to be $B/3\mathcal{R}$. This last expression can be quickly derived by considering the pressure jump across the drop interface in the contact region, approximating the internal pressure by $2\sigma/R_0$, and calculating the external pressure by balancing the drop's weight and the total reaction force. Since $B = O(\mathbb{W}e^{1/2})$ from the conservation of energy, the maximum relative contact area scales as $\mathbb{W}e^{1/2}/\mathcal{R}$, the square root of the rescaled Weber number. Therefore, our model should break down when $\mathbb{W}e/\mathcal{R}^2 \approx 1$, i.e., when the impact speed becomes sufficiently high, or the substrate curvature sufficiently close to that of the drop, that the contact area becomes comparable to the drop area and the nonlinear effects become important. Little can be said at this point about the drop dynamics in the $\mathbb{W}e/\mathcal{R}^2 > 1$ regime.

Our quasi-static and numerical models clearly indicate that both the contact time (Fig. 7) and the coefficient of restitution (Fig. 9) increase logarithmically with decreasing values of the rescaled Weber number. The reason for both of these effects is the logarithmic divergence of the static shape for small contact areas (see Eq. (10)), which allows the drop to localize its deformation to a small region around the contact area. Viscous dissipation is then similarly localized and therefore restricted in its total amount, leading to a higher coefficient of restitution. On the other hand, the divergence of the static shape allows the drop to deform further with the same increase in total surface energy, reducing the effective spring constant associated with the deformation and thus increasing the rebound time. From (36), we see that the total mechanical energy of the drop scales as $\rho R_0^5 \ln^2(1/B)\dot{B}^2$, while the kinetic energy associated with the internal circulation is only of order $\rho R_0^5 \dot{B}^2$ (see Eq. (28)). Viscosity can only dissipate the latter component, with viscous dissipation scaling as $\mu R_0^3 \dot{B}^2$ (29). Integrating the dissipation over the contact time, which scales like $(\rho R_0^3/\sigma)^{1/2} \ln(1/B)$, we thus expect the relative energy loss during rebound to scale as $\mathbb{O}h/\ln(1/B) \sim \mathbb{O}h/\ln(1/\mathbb{W}e)$ (see Fig. 9).

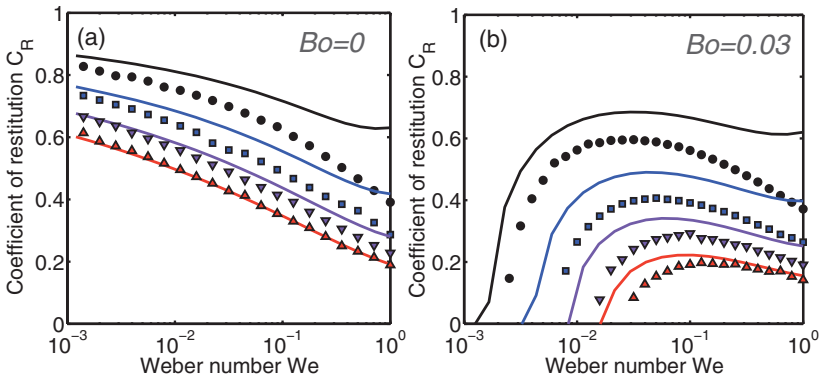

FIG. 9. The dependence of the coefficient of restitution C_R on the Weber number $\mathbb{W}e = \rho R_0 V_{in}^2/\sigma$ with (*a*) and without (*b*) gravity, for a drop impacting a flat substrate ($\mathcal{R} = 1$). Results of the quasi-static model (38) (solid lines) and the full numerical model (42) (points) are shown for four values of the Ohnesorge number $\mathbb{O}h = \mu/\sqrt{\rho\sigma R_0}$: $\mathbb{O}h = 0.1$ (•), $\mathbb{O}h = 0.2$ (■), $\mathbb{O}h = 0.3$ (▼), and $\mathbb{O}h = 0.4$ (▲).

The effects of gravity have also been studied by Okumura *et al.*,[17] whose experimental results are shown in Fig. 8, together with our analytical expression (44), the quasi-static model (38), and the numerical model (42). The quasi-static model stays within 12% of the experimental data for the whole range of Weber numbers considered. As a reference, we include the line for zero gravity. We see that the increase in contact time with decreasing $\mathbb{W}e$ found experimentally by Okumura *et al.* may be attributed to the effects of small $\mathbb{W}e$ and not to gravity.

B. Coefficient of restitution

The quasi-static model (38) provides a fast way of estimating the coefficient of restitution. The velocity of the droplet center of mass can be obtained from (38) and (39) as $b_1'(B)\dot{B}$, giving

$$C_R = \frac{b_1'(B(\tau_c))\dot{B}(\tau_c)}{b_1'(B(0))\dot{B}(0)}, \tag{45}$$

where τ_c is the contact time. The dependence of C_R on Ohnesorge number, Weber number, and Bond number for a flat surface ($\mathcal{R} = 0$) is shown in Fig. 9. In order to check the accuracy of the quasi-static model, we include the results of the full numerical model (42). As expected, C_R decreases uniformly with increasing viscosity. Nevertheless, as $\mathbb{O}h \to 0$, it does not approach 1, but a somewhat smaller value due to a transfer of the kinetic energy into the vibrational modes, as observed by Richard and Quéré. This transfer cannot be captured by the quasi-static model and therefore the model overestimates C_R for low $\mathbb{O}h$ and high $\mathbb{W}e$. The match improves with decreasing $\mathbb{W}e$ and increasing viscosity. In absence of gravity, C_R uniformly increases with decreasing Weber number, but when $\mathbb{B}o > 0$, it reaches a peak and then sharply drops to zero near $\mathbb{W}e \approx \mathbb{B}o \cdot \mathbb{O}h$ as the drop fails to detach. Both of these phenomena are captured well by our model.

V. DISCUSSION

We have presented a conceptually simple theoretical model for the dynamics of a drop impacting a rigid substrate, which is valid when the drop deformation remains small and the effects of contact line dynamics and dissipation in the surrounding gas can be neglected. It has allowed us to characterize the effects of both the Weber number and substrate curvature on the dynamics. The form of the equation of motion suggests that in the small deformation limit these two effects are captured by a single nondimensional group—square root of the rescaled Weber number $\mathbb{W}e^{1/2}/\mathcal{R}$, where $\mathcal{R} = 1 - R_0/R_2$, which is proportional to the ratio of the maximum contact area to the drop's total area. When $\mathbb{W}e^{1/2}/\mathcal{R} < 0.3$, the dynamics can be approximated by a simple differential Eq. (40), which can be interpreted as a logarithmic spring. The model reproduces all the qualitative

features of the drop dynamics and is in good quantitative agreement (within 10%) with previously reported experiments and numerical results when $\mathbb{W}e^{1/2}/\mathcal{R} < 0.1$. It removes the need to deal with the complicated interaction between the drop and the impacted substrate considered in the usual numerical simulations, and is very fast to solve numerically. The relatively simple form of the equation of motion (40) also allows analytical treatment in the $\mathbb{W}e^{1/2}/\mathcal{R} \ll 1$ limit.

Both the coefficient of restitution and the contact time of the impacting drop increase with decreasing rescaled Weber number. For a fixed impact speed, the rescaled Weber number is reduced by decreasing the radius of curvature of the substrate. We note that the wettability of the surface will in general depend not only on the rescaled Weber number through its influence on the impact dynamics, but also on the surface microstructure and its influence on the sustenance of the lubricating air layer. The spacing and shape of the microstructure for optimal water-repellency has been considered in the context of static drops.[29–32] An equivalent study of optimal water-repellent design in this dynamic setting, wherein both micro- and macrostructure are important, is left for future consideration.

Approximating the shape of a deformable substrate by its quasi-static shape would presumably allow one to extend the quasi-static model presented here to a more general scenario of liquid drops impacting a liquid bath. Such a model would prove useful in rationalizing the coalescence criteria for impacting liquid drops[33] and the phase diagrams of drops bouncing on a vertically vibrated liquid bath.[34,35] The development of such models will be the subject of future work.

[1] L. L. English, "Some properties of oil emulsions influencing insecticidal efficiency," Bull. Illinois Nat. Hist. Surv. **17**, 233–259 (1928).
[2] W. Moore, "Spreading and adherence of arsenical sprays," Minnesota Agri. Exp. Station Tech. Bull. **2**, 1–50 (1921).
[3] F. Wilcoxon and A. Hartzell, "Some factors affecting the efficiency of contact pesticides. I. Surface forces as related to wetting and tracheal penetration," Contr. Boyce. Thompson Inst. **3**, 1–12 (1931).
[4] H. Wijshoff, "The dynamics of the piezo inkjet printhead operation," Phys. Rep. **491**, 77–177 (2010).
[5] Q. Zhou, N. Li, X. Chen, T. Xu, S. Hui, and D. Zhang, "Liquid drop impact on solid surface with application to water drop erosion on turbine blades, Part II: Axisymmetric solution and erosion analysis," Int. J. Mech. Sci. **50**, 1543–1558 (2008).
[6] D. Quéré, "Wetting and roughness," Annu. Rev. Mater. Res. **38**, 71–99 (2008).
[7] J. W. M. Bush, D. L. Hu, and M. Prakash, "The integument of water-walking arthropods: Form and function," Adv. Insect Physiol. **34**, 117–192 (2008).
[8] P. G. Gennes, F. Brochard-Wyart, and D. Quéré, *Capillarity and Wetting Phenomena: Drops, Bubbles, Pearls, Waves* (Springer, New York, NY, 2003).
[9] A. Yarin, "Drop impact dynamics: Splashing, spreading, receding, bouncing. . . " Annu. Rev. Fluid. Mech. **38**, 159–192 (2006).
[10] Z. Wang, C. Lopez, A. Hirsa, and N. Koratkar, "Impact dynamics and rebound of water droplets on superhydrophobic carbon nanotube arrays," Appl. Phys. Lett. **91**, 023105 (2007).
[11] T. Gilet and J. W. M. Bush, "Droplets bouncing on a wet, inclined surface," Phys. Fluids **24**, 122103 (2012).
[12] S. Dorbolo, D. Terwagne, N. Vandewalle, and T. Gilet, "Resonant and rolling droplets," New J. Phys. **10**, 113021 (2008).
[13] G. Foote, "The water drop rebound problem: Dynamics of collision," J. Atmos. Sci. **32**, 390–402 (1975).
[14] A. Gopinath and D. Koch, "Collision and rebound of small droplets in an incompressible continuum gas," J. Fluid Mech. **454**, 145–201 (2002).
[15] D. Richard and D. Quéré, "Bouncing water drops," Europhys. Lett. **50**, 769–775 (2000).
[16] D. Richard, C. Clanet, and D. Quéré, "Contact time of a bouncing drop," Nature (London) **417**, 811 (2002).
[17] K. Okumura, F. Chevy, D. Richard, D. Quéré, and C. Clanet, "Water spring: A model for bouncing drops," Europhys. Lett. **62**, 237–243 (2003).
[18] Lord Rayleigh, "On the capillary phenomena of jets," Proc. R. Soc. London, Ser. A **29**, 71 (1879).
[19] A. K. Chesters, "An analytical solution for the profile and volume of a small drop or bubble symmetrical about a vertical axis," J. Fluid Mech. **81**, 609–624 (1977).
[20] P. G. Smith and T. G. M. van De Ven, "Profiles of slightly deformed axisymmetric drops," J. Colloid Interface Sci. **97**, 1–8 (1984).
[21] M. E. R. Shanahan, "Profile and contact angle of small sessile drops," J. Chem. Soc. **80**, 37–45 (1984).
[22] S. W. Rienstra, "The shape of a sessile drop for small and large surface tension," J. Eng. Math. **24**, 193–202 (1990).
[23] D. C. Morse and T. A. Witten, "Droplet elasticity in weakly compressed emulsions," Europhys. Lett. **22**, 549–555 (1993).
[24] S. Chandrasekhar, *Hydrodynamic and Hydromagnetic Stability* (Clarendon, Oxford, 1961), pp. 466–477.
[25] C. Miller and L. Scriven, "The oscillations of a fluid droplet immersed in another fluid," J. Fluid Mech. **32**, 417–435 (1968).
[26] A. Prosperetti, "Viscous effects on perturbed spherical flows," Q. Appl. Math. **35**, 339–352 (1977).
[27] A. Prosperetti, "Free oscillations of drop and bubbles: The initial-value problem," J. Fluid Mech. **100**, 333 (1980).
[28] B. J. Torby, *Advanced Dynamics for Engineers* (Holt, Rinehart, and Winston, New York, NY, 1984), p. 271.
[29] N. A. Patankar, "Mimicking the lotus effect: Influence of double roughness structures and slender pillars," Langmuir **20**, 8209–8213 (2004).

[30] A. Otten and S. Herminghaus, "How plants keep dry: A physicist's point of view," Langmuir **20**, 2405–2408 (2004).
[31] D. Quéré and M. Reyssat, "Non-adhesive lotus and other hydrophobic materials," Philos. Trans. R. Soc. London, Ser. A **366**, 1539–1556 (2008).
[32] Z. Guo and W. Liu, "Biomimic from the superhydrophobic plant leaves in nature: Binary structure and unitary structure," Plant Sci. **172**, 1103–1112 (2007).
[33] Y. Couder, E. Fort, C. Gautier, and A. Boudaoud, "From bouncing to floating: Noncoalescence of drops on a fluid bath," Phys. Rev. Lett. **94**, 177801 (2005).
[34] A. Eddi, D. Terwagne, E. Fort, and Y. Couder, "Wave propelled ratchets and drifting rafts," Europhys. Lett. **82**, 44001 (2008).
[35] S. Protiére, A. Boudaoud, and Y. Couder, "Particle-wave association on a fluid interface," J. Fluid Mech. **554**, 85–108 (2006).